Thin Sheet Conductance Models from Geomagnetic Induction Data: Application to Induction Anomalies at the Transition from the Bohemian Massif to the West Carpathians

Václav Červ[a] (vcv@ig.cas.cz), Světlana Kováčiková[a], Michel Menvielle[b] and Josef Pek[a]

[a]Inst. Geophys., Acad. Sci. Czech Rep., v.v.i., Prague, Czech Rep.
[b]CEETP CNRS, Saint Maur des Fosses, France

Abstract

Thin sheet approximation of Earth's conductive structures made it possible to quantitatively estimate effects of lateral conductivity variations in the Earth long before full 3-D electromagnetic modeling was practicable. The thin sheet approach is still useful when induction data with limited vertical resolution are to be interpreted on a surface. It especially refers to collections of long period induction arrows across large areas and geological units. For this purpose, inverse procedures, both linearized and stochatic, for a conductance distribution in a thin sheet have been suggested recently. We present a stochastic Monte Carlo inversion of geomagnetic induction data based on the bayesian formulation of the inverse problem. An example of the inversion of practical induction data from the transition zone between the Bohemian Massif and the West Carpathians suggests that an SW-NE anomalous induction zone observed above the eastern slopes of the Bohemian Massif admits explanation in terms of a phantom effect due to the superposition of fields of the strong SE-NW Carpathian conductivity anomaly to the east with NW-SE to W-E trending conductivity zones to the west that conform with the fault pattern of the eastern Bohemian Massif.

1 Introduction

Regional geoelectrical information on the contact zone between the Variscean Bohemian Massif and the Alpine Western Carpathians is mainly available from long-period geomagnetic transfer functions. Magnetotelluric data and broadband electromagnetic induction experiments are scarce in the region, mainly because of high level of the civilization noise all over the area, and also because of the lack of instrumentation in the past. Only recently, magnetotelluric experiments have been carried out in some subareas of the region, mainly for commercial targets (e.g., Vozár, 2005).

Long-period geomagnetic induction data covering a period band of about one decade in the range of thousands of seconds cannot provide detailed geoelectrical information on structures beneath the region of interest. They are, however, suitable characteristics to be used to model large-scale horizontal conductivity distribution in the Earth's crust or lithosphere, and thus to indicate regional lateral conductivity anomalies that are responsible for the observed induction pattern over the area under study. With data at periods of the order of thousands of seconds, with penetration depths starting at several tens of km for standard conditions of the continental lithosphere, a quasi 3-D thin sheet approximation of crustal conductivity structures is a reasonable induction model (e.g., Vasseur and Weidelt, 1977). The thin sheet approximation largely reduces the computational demands of the modeling procedure as compared with a full 3-D treatment and, moreover, bypasses some intrinsic difficulties of dealing with the geomagnetic induction data alone, especially their low sensitivity with respect to the normal layered background of the model.

Recently, two methods of inversion of geomagnetic induction data for conductances in a thin sheet have been developed, one based on the non-linear conjugate gradient technique (Wang and Lilley, 2002) and the other on a Bayesian approach with Markov chain Monte Carlo (MCMC) method used for a stochastic sampling process (Grandis, 2002). In this contribution, we are using the latter approach to analyze conductance distributions which are compatible with the geomagnetic induction data in the West Carpathians region and at its transition to the Bohemian Massif on the territories of the Czech Republic, Slovakia and Poland.

More specifically, the data base of this study are induction response data at 150 field stations that were published earlier (Praus and Pěčová, 1991) covering the Bohemian Massif (BM), the Brunovistulicum (BV), and the West Carpathian region (WCP) and re-analyzed in (Pěčová and Praus, 1996). Spatial distribution of both the in-phase and the out-of phase induction vectors, contour maps of individual transfer functions (TF) and contour maps of anomalous

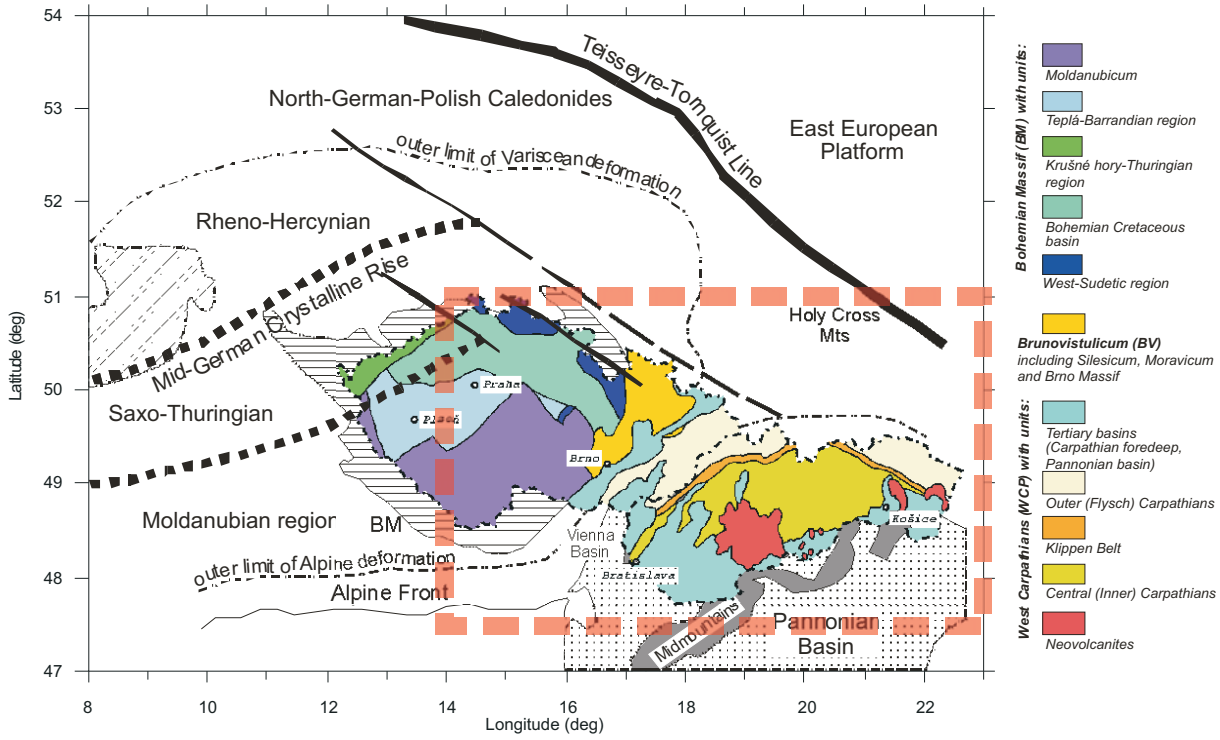

Figure 1: Geological scheme of the region of Central Europe relevant to our modeling study. The dashed-line rectangle shows the region in which the inversion for a laterally variable conductance distribution in a thin sheet is carried out.

vertical field that were generated from the TF's by the hypothetical field of different polarizations and systems of internal anomalous currents indicate the existence of two zones of anomalous induction at the eastern margin of the BM and near the boundary of the Carpathian plate (Kováčiková *et al.*, 1997). The previous analyses, and the recent one performed by a new approach to imaging the induction data of the Wiese vectors at almost 1800 localities covering mainly the Central European area (Wybraniec *et al.*, 1999) suggest that these anomalies might be connected with the North-German-Polish anomalous zone, representing an important part of the Trans-European Suture Zone (TESZ). The analysis of certain models of electrical conductivity distribution is performed to fit the anomalous features of the induction response data over the Central European area, specifically zones of anomalous induction in the eastern margin of the BM, across the entire block of the BV and near the margin of the Carpathian tectonic plate.

The structure of the article is as follows: In Section 2, we give a short overview of the principal geological units of the region under study. Section 3 briefly summarizes the geoelectrical features of the region previously inferred from the geomagnetic induction data in the region. In Section 4, we formulate the thin sheet model used in the inversion. The principles of the Bayesian inversion of the geomagnetic induction data for the conductance distribution in the thin sheet are presented in Section 5. Section 6 then summarizes outputs of the Bayesian inversion for the induction data over the BM/BV/WCP region with indications on possible correlations of the conductance model with regional geological structures.

2 Geological context of the induction studies

Fundamental elements of the central European geological structure that are relevant to our modeling experiment are schematically displayed in Fig. 1 together with the major geological units over the Czech and Slovak Republics covered by induction response data involved in the modeling process.

(i) The Tornquist-Teisseyre tectonic zone (TTZ) constitutes one substantial part of a number of fault zones and sutures found within the Trans-European Suture Zone (TESZ) that represents the most important geological boundary in Europe separating mobile Phanerozoic western terranes (Meso-Europe) from the Precambrian east European Craton. It is as clearly defined in the deep lithosphere as in the upper crust, Moho depths increase across this zone from 30 km beneath Variscan Europe to 45 km beneath the East European Craton. In contrast to the relatively cold eastern craton relatively high heat flow characterises Western Europe.

(ii) The Bohemian Massif (BM) represents the easternmost consolidated block of the Variscan branch of the European Hercynides (Meso-Europe) that builds up Bohemia and the western part of Moravia. The major elements of

the BM are several SW-NE trending zones separated usually by deep-seated faults, which are reflected in the results of the deep seismic profiling, in the gravity, geomagnetic and heat flow maps (Suk *et al.*,1984). The fault structures are essentially parallel with the boundaries of individual Hercynian zones. The intersection of these zones with the second order system of NW-SE trending faults is responsible for the complicated block structure of the BM.

(iii) The Carpathians belong to the young Tertiary Alpine-orogenic belt and they constitute the NE branch of the Alpides. Their boundary with the Eastern Alps runs along the Danube Valley. The northern boundary with the East European Platform is defined by the erosive margin of the flysch nappes. Our model covers the West Carpathians (WCP) and we distinguish here the inner (central) Carpathians, the Klippen zone, the outer (Flysch) Carpathians and the Carpathian foredeep (Fig. 1, dashed-line rectangle).

(iv) The Brno unit, termed recently the Brunovistulicum (BV) (Dudek, 1980; Suk, 1995) lies in between those previously mentioned structural elements. The BV unit is assumed to be an independent geological structure forming the Precambrian (Cadomian) basement (Palaeo-Europe) of both the eastern part of the Hercynides (Variscides) of the BM and the Alpides, i.e. of the WCP in Moravia. Recent geophysical and geological data have shown that the BV and the whole Moravian block occupy a highly independent position and form a separate geological unit belonging probably to the Fenno-Sarmatian Platform (Dudek, 1980).

3 Geoelectrical data and features of the region

3.1 The data

The experimental data were collected in 1970's and 1980's in a series of field experiments organized in co-operation with Czech, Slovak and Polish colleagues. The field measurements consisted in analogue recordings of magnetic transient variations at alltogether 150 temporary field sites over an area of about 500×250 km^2. They were analysed in terms of induction arrows (Wiese, 1962). At each station, in-phase and out-of phase induction arrows have been estimated for periods in the range of 1200 to 5840 s. They correspond to the real and imaginary components of single-station transfer functions between the horizontal and vertical components of the transient magnetic field at the station. A sample of the real and imaginary induction arrows at a particular period of $T = 3860$ s is presented in Fig. 2.

3.2 Major conductivity anomalies

As the magnetic Z-component is known to be highly sensitive to laterally inhomogeneous distribution of the internal electrical conductivity, maps of these vectors provide us with a view of the changing anomalous behaviour of the Z-variation as function of frequency and location. Reversals of the arrows distinguish zones of anomalous induction, which often mark important geological features such as contacts between blocks with different geological histories of development, zones of past and recent tectonic activities, collision zones and etc. A qualitative analysis of the maps of induction arrows led to evidence two major conductivity anomalies in the area under study. Quantitative modeling allowed to characterize the conductivity distribution in the lithosphere that accounts for the observed induction arrows.

The Carpathian anomaly, WCA The induction vectors across the WCP region show a clear perpendicular orientation with respect to a general trend of the anomalous induction zone localized along the external margin of the Carpathians Mts. chain (see WCA in Fig. 2. They show almost a perfect 180^o reversals of their azimuths above the anomalous induction zone. In the WCP, modules of the induction vectors situated to the south from the zero line are by about 25-50% larger than the corresponding induction vectors located to the north of the anomaly. The Carpathian

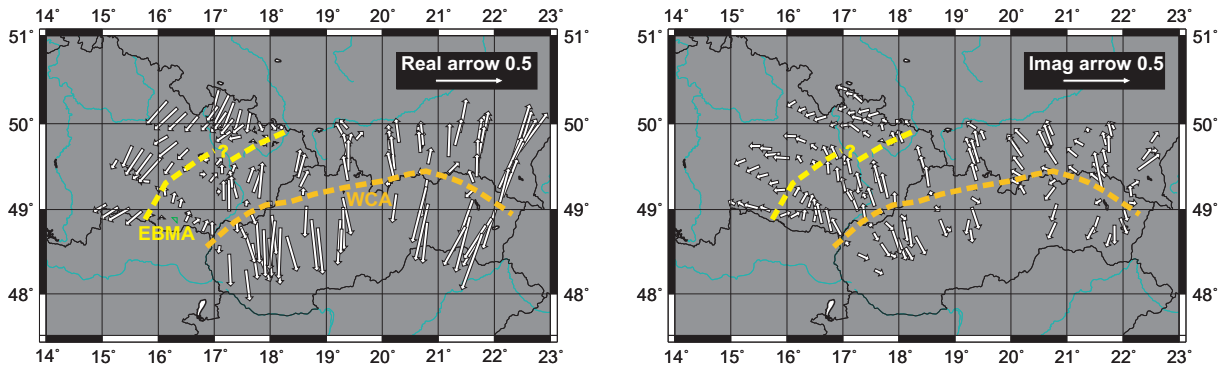

Figure 2: Sample of experimental real and imaginary induction arrows in the BM/BV/WCP region for the period of 3860 s, with two main regional conductivity anomalies indicated, the West Carpathian conductity anomaly (WCA) and the conductivity anomaly on the eastern margin of the Bohemian Massif (EBMA).

geoelectrical anomaly is constrained by the presence of high-conductivity rock series at depth of 10-25 km in different segments of the orogen. Different geological models explaining the presence of highly conductive rocks or solutions as sources of the anomalies have been suggested. The role of altered and/or fractured rocks, saturated with hot mineral waters, as well as the proximity of anomaly sources to boundaries of different crustal blocks, including those between the Carpathians and adjacent platforms, have been taken into account (Ádám and Pospíšil, 1984; Jankowski *et al.*, 1984; 1991; 2008; Hvoždara and Vozár, 2004). Other authors discuss possible connection between the Carpathian anomaly and the presence of metamorphosed coal bearing Carboniferous strata beneath the orogen or relation to the graphitized rocks occurring close to the boundaries of crustal blocks (Glover and Vine, 1992; Glover and Vine, 1995; Żytko, 1997).

The EBMA anomaly The induction vectors on the eastern margin of the BM are distinguished by the vectors oriented predominantly parallel to the general SW-NE trend of the anomalous zone. Also the reversal of the azimuths at the anomalous zone is rather poorly developed, only sudden changes of azimuths are observed at individual profiles. These facts are clear indications of a 3-D character of the conductivity distribution. The EBMA has been generally attributed to processes in the the subduction of the eastern margin of the BM beneath the WCP plate, but precise induction processes for generating the peculiar 3-D features of this anomaly are still unknown (e.g. Kováčiková *et al.*, 2005). Speculating on the physical/geological sources of the anomaly may thus be premature.

3.3 Results from numerical modeling

From the equivalent current systems (Červ *et al.*, 1997) it was concluded that the source depth of the induction anomalies can be about 18 km in the WCP region and about 10 km in the EBM/BV. These estimates are suggesting the source of the anomalies at shallower depth than those obtained previously by separating the magnetic field variations into internal and external parts (Pěčová and Praus, 1996) and applying the line current approximation (Jankowski *et al.*, 1985).

2-D models for induction vectors along the profiles crossing the WCP are summarized in (Jankowski *et al.*, 1985). The models featured anomalous bodies with a cross-section$\times$ conductivity parameter of the order of 10^7 to 10^8 Sm, with the top of the bodies at depths beneath 12-15 km. In (Jankowski *et al.*, 1991) the 2-D modeling was used for simultaneous modeling of the induction vectors and apparent resistivities, collected in a series of sites in the Polish section of the Carpathian Foredeep. In the latter models, the source of the WCA was situated at shallower depths, less than about 10 km, and hypothesized to be related to deep sediments of the Carpathian Foredeep. The 2-D inversion on the Carpathian data was firstly used in (Červ and Pek, 1981). The geoelectrical structural model along the DSS profile No VI, crossing the BM, BV and WCP, based on the MT and MV results was presented in (Červ *et al.*, 1984).

3.4 Depth of the asthenosphere

The electrical asthenosphere, if present, is an additional structural feature that can affect the induction data especially at long periods. In the model derived from the P-wave residuals for the Bohemian Massif the depth of the lithosphere-asthenosphere transition zone are between 90 and 140 km (Babuška *et al.*, 1988). From MT sounding a layer of increased electrical conductivity attributable to the asthenosphere was interpreted at depth between 100 and 150 km (Červ *et al.*, 1984).

The most likely depth of the conducting layer in the upper mantle in the Pannonian Basin region are between 60 and 85 km in the central part of the depression. The depths seem to increase towards the flanks of the basin to about 100 km (Ádám, 1976). In some parts (Rába-Rožnava tectonic line) the thickness of the litosphere reduces to even less than 60km (Ádám, 1988). The regions of lithosphere thinning penetrate from the Pannonian Basin into inner parts of the WCP in several promontories. In the thinned part of the lithosphere in the West Carpathians the lithosphere-asthenosphere transition zone is at the depth 90-120 km (Červ *et al.*, 1984).

A gradual increase of the lithosphere thickness to 140-180 km occurs in the Outer Carpathians and father towards the margin of the East European Platform (Praus *et al.*, 1990). In the Alps the depth of the asthenosphere varies from 100 to 200 km (Praus *et al.*, 1990).

4 A possible thin sheet model

In the subsequent inversion for a laterally non-uniform conductance, we will use a thin sheet model formally defined as follows:

Let us consider a model consisting in a heterogeneous thin sheet at the surface of or embedded in a 1-D medium, hereafter called normal model. The normal model is defined by the conductivities $\sigma_n(\mathbf{r})$ at any point $\mathbf{r}$. In the thin sheet, the actual conductivity $\sigma(\mathbf{r})$ differs from the normal one in a domain of interest Ω. Inside Ω, $\sigma_a(\mathbf{r})$ denotes the

difference $\sigma(\mathbf{r}) - \sigma_n(\mathbf{r})$: $\sigma_a(\mathbf{r})$ is the anomalous conductivity that is zero outside Ω. Solutions of the forward and inverse problems have already been published for such a model. They are briefly recalled in the next section.

With regard to the experimental geomagnetic TF's available, several aspects of the thin sheet model must be considered. First, the validity of the thin sheet hypothesis must be assessed. We assume that the anomalous electrical targets are localized mainly in the crust. Penetration depths for typical continental crustal sections should not be less than about 50 km in the period range of thousands of seconds (corresponds to the resistivity of 10 Ωm and period of 1000 s). Thus, the anomalous zone of 20-30 km below the Earth's surface can be reasonably (though, may be, not completely unquestionably for highly conductive anomalous zones) approximated by a thin sheet. According to Bruton (1994), the size of the square tiles a used to discretize the anomalous subdomain Ω of the sheet should meet the condition $a\omega\mu S_{\max} \ll 1$. For the most extreme parameters in our models, say $T_{\min} = 1200$ s and $S_{\max} = 5000$ siemens, the size of the tiles should be much less than about 30 km. We typically use tiles with $a = 20$ to 25 km in our models, which meets the Bruton's condition for most of the model situations.

The second aspect is the depth of the thin sheet. As we are not able to employ a multiple sheet model in the inversion at present, we use a single thin sheet that integrates all the conductivity anomalies from the surface down to the crust. Thus, the sheet is situated on the surface of the Earth in our experiments. This may result in increased misfit, especially in imaginary induction arrows, if the anomalous current flow deep in the crust.

The third aspect is the embedding normal structure. Due to large differences of the depth vs. resistivity sections of the two main region of our study, the BM and the WCP with the adjacent Pannonian Basin, we cannot suggest any single 1-D normal model down to the asthenospheric depths for the whole region. Therefore, we simplified the normal model into a two-layer structure with a poor conductor resistivity of several hundreds of Ωm up to 1000 Ωm) underlaid by a more conductive asthenosphere with resistivity within the range of 100-500 Ωm. The effect of the topography of the asthenospheric layer was checked independently by a 3-D modeling experiment with seismic data (Praus *et al.*, 1990) taken to approximate the top of the asthenosphere. The checks showed that the effect of the asthenosphere is negligible in induction arrows for periods of the order of thousands of seconds unless the resistivity of the asthenosphere is less than about 10 Ωm.

5 Bayesian Monte Carlo Markov Chain thin sheet inversion

We present in this section the Bayesian Monte Carlo Markov Chain (MCMC) method we used to solve the inverse problem. For the sake of self-completeness, let us first briefly recall basic notions concerning Bayesian inversion and Markov chains behaviour. The readers are referred to Roussignol *et al.* (1993), Menvielle and Roussignol (1995), and Grandis *et al.* (1999; 2002), and references therein for more details.

5.1 The Bayesian approach

Let the a priori knowledge be the information available on the model before processing the data, and the a posteriori knowledge the information available after processing the data. A priori and a posteriori distributions account in a probabilistic way for the a priori and a posteriori knowledge respectively. In the Bayesian context, solving the inverse problem thus comes down to determining the a posteriori knowledge by updating the a priori knowledge with the information gleaned from the data (Box et Tiao, 1973; Berger, 1985; Press et al., 1989).

Solving the inverse problem first requires the direct problem to be solved. Let F be the direct problem function which enables computation of the observations $\mathbf{d}$ for a model $\mathbf{m}$. Assuming that the error $\delta\mathbf{d}$ is only related to the data acquisition, it becomes

$$\mathbf{d} = F(\mathbf{m}) + \delta\mathbf{d}$$

The a priori knowledge is given by a probability distribution function (*pdf*) $P_0(\mathbf{M} = \mathbf{m} \,|\, \mathbf{M} \in \mathcal{M})$ defined on the set of possible models $\mathcal{M}$. The a posteriori probability for the parameter vector $\mathbf{M}$ to take the value $\mathbf{m}$ given the observations $\mathbf{d}$ is given by Bayes' formula (Bayes, 1763; also see, e.g., Bolstad, 2004, for a more modern treatment). Noting $P(\mathbf{M} = \mathbf{m} \,|\, \mathbf{D} = \mathbf{d}, \mathbf{M} \in \mathcal{M})$ the conditional probability of $\mathbf{M}$ given $\mathbf{D}$, and assuming that the error $\delta\mathbf{d}$ is gaussian with standard deviation τ, it becomes

$$P(\mathbf{M} = \mathbf{m}|\mathbf{D} = \mathbf{d}, \mathbf{M} \in \mathcal{M}) = \frac{\exp\left[-\dfrac{||F(\mathbf{m}) - \mathbf{d})||^2}{2\tau^2}\right] P_0(\mathbf{m})}{\displaystyle\sum_{\mathbf{m}\in\mathcal{M}} \exp\left[-\frac{||F(\mathbf{m}) - \mathbf{d})||^2}{2\tau^2}\right] P_0(\mathbf{m})} \tag{1}$$

The value $\mathbf{d}$ of the random vector $\mathbf{D}$ corresponds to the observed data. Since $\mathbf{d}$ is not modified during the inversion process, we will from now on omit $\mathbf{D}$ in the expression of the probability distributions and denote the a posteriori *pdf* $P(\mathbf{M} = \mathbf{m}|\mathbf{D} = \mathbf{d}, \mathbf{M} \in \mathcal{M})$ simply by $\Pi(\mathbf{m})$.

The normalization constant, which appears in the denominator of eq. (1) is a sum over the set of possible models, the dimension of which is very large: for instance, it is equal to $M \times L$ for models with M parameters that can each take on L different values. It is actually very difficult, if not impossible to estimate directly. We choose to use a Monte Carlo Markov Chain (MCMC) simulation method to achieve this estimation.

5.2 Markov chains

In order to estimate the *pdf* $\Pi(\mathbf{m})$, let us define a Markov Chain on the set $\mathcal{M}$ of possible models that have $\Pi(\mathbf{m})$ as invariant probability. The marginal *pdf*'s of $\Pi(\mathbf{m})$ will be estimated by empirical averages from simulations of the Markov Chain.

Consider a system which can take a certain number of states and evolves at random with time. At a given time, the state of the system can be described as a random variable $\mathbf{M}$, the values of which, $\mathbf{m}$, belong to $\mathcal{M}$. The system is a Markovian process if, at any time, its future evolution depends only on its present state. It means that a Markovian system depends only on its past through its present state. Markov chains are a particular class of Markovian processes such that (i) the set $\mathcal{M}$ is finite or countable, and (ii) the successive times for the evolution are denoted by integers. A series $\{\mathbf{M}(n), n = 0, 1, 2, \ldots, N\}$ of random variables with values in a finite or countable space is then a Markov chain if the state of the system at the time $n + 1$, $\mathbf{M}(n + 1)$, depends only on its past through the state of the system at time n, $\mathbf{M}(n)$. The behaviour of a Markov chain is defined by the set of its transition probabilities,

$$P_n(\mathbf{m}, \mathbf{m}') = P\left(\mathbf{M}(n+1) = \mathbf{m}' | \, \mathbf{M}(n) = \mathbf{m}\right),$$

where $\mathbf{m}$ and $\mathbf{m}'$ belong to $\mathcal{M}$. If (i) the transition probabilities do not depend on time n, (ii) $\mathcal{M}$ is finite, and (iii) each possible state can be reached from any other, the chain is a homogeneous ergodic aperiodic Markov chain, and there exists one, and only one probability density function Π on $\mathcal{M}$ which is invariant for the Markov chain. When n increases towards infinity, the behavior of ergodic Markov chains is such that the average fraction of time at which the chain is at a state $\mathbf{m}$ ($\mathbf{m} \in \mathcal{M}$) tends towards the invariant probability of $\mathbf{m}$, i.e. $\Pi(\mathbf{m})$.

Methods for Bayesian inversion with Markov chains has been proposed for the 1-D magnetotelluric (Grandis *et al.*, 1999) and DC problems (Schott *et al.*, 1999) with the a priori of smooth variation of resistivity with depth, and for the thin sheet approximation (Roussignol *et al.* 1993; Grandis, 1994; Grandis *et al.*, 2002). The present analysis of crustal conductivity over the transition from the Bohemian Massif to the West Carpathians relies on the inversion of induction arrows using the latter method, which is briefly described in the following sections.

5.3 The thin sheet forward problem

Let us consider a model consisting of a heterogeneous thin sheet at the surface of or embedded in a 1-D medium, specified in detail in the first two paragraphs of Section 4 above. Let $\mathbf{E}(\mathbf{r}, \omega, \sigma)$ and $\mathbf{H}(\mathbf{r}, \omega, \sigma)$ be the time Fourier transforms of the electric and magnetic field at point $\mathbf{r}$ and circular frequency ω, $\omega = 2\pi/T$, T period, for the actual conductivity structure σ. Using the Green kernel method, we can rewrite basic equations of electromagnetism as (Weidelt, 1975)

$$\mathbf{E}(\mathbf{r}, \omega, \sigma) = \mathbf{E}_n(\mathbf{r}, \omega) - i\omega\mu \int_\Omega \sigma_a(\mathbf{r}') \, \mathbb{G}(\mathbf{r}, \mathbf{r}', \omega) \, \mathbf{E}(\mathbf{r}', \omega, \sigma(\mathbf{r}')) \, d^3\mathbf{r}', \tag{2}$$

$$\mathbf{H}(\mathbf{r}, \omega, \sigma) = \mathbf{H}_n(\mathbf{r}, \omega) + \int_\Omega \sigma_a(\mathbf{r}') \, \mathrm{curl}(\mathbb{G}(\mathbf{r}, \mathbf{r}', \omega)) \, \mathbf{E}(\mathbf{r}', \omega, \sigma(\mathbf{r}') \, d^3\mathbf{r}', \tag{3}$$

at any point $\mathbf{r}$ and any frequency ω. The quantity μ is the magnetic permeability of the vacuum in our models. $\mathbb{G}(\mathbf{r}, \mathbf{r}', \omega)$ is a 3×3 complex matrix, named Green kernel, and represents the Fourier transform at frequency ω of the electric field created at point $\mathbf{r}$ by a unit dipole $\boldsymbol{\delta}(\mathbf{r}')$ located at point $\mathbf{r}'$ (Morse and Feshbach, 1953), $\mathrm{curl}(\mathbb{G}(\mathbf{r}, \mathbf{r}', \omega))$ is a 3×3 complex matrix obtained by taking the curl at point $\mathbf{r}$ of the field of the column vectors of the matrix $\mathbb{G}(\mathbf{r}, \mathbf{r}', \omega)$.

A numerical solution of the forward problem has been first proposed by Vasseur and Weidelt (1977) for a superficial thin sheet. The Vasseur and Weidelt's (1977) approach can be extended to a thin sheet at any depth below the surface. The code was made operational by Tarits (1989). These solutions are based upon a digitization of Ω in K small square cells P_k, $k = 1, \ldots, K$, in which conductivities, Green kernels, electric and magnetic fields are nearly constant. Let $S(P_k)$ and $S_n(P_k)$ be the actual and normal integrated conductivities (i.e. conductances) of the cell P_k, and $S_{ak} = S(P_k) - S_n(P_k)$, $k = 1, \ldots, K$, the anomalous conductance of P_k. Then basic equations become, using the

same notations for the sake of simplicity,

$$\mathbf{E}(\mathbf{r},\omega,S) = \mathbf{E}_n(\mathbf{r},\omega) - i\omega\mu \sum_k S_{ak}\, \mathbb{G}(\mathbf{r},P_k,\omega)\, \mathbf{E}(P_k,\omega,S(\mathbf{r}'))\, |P_k|, \quad (4)$$

$$\mathbf{H}(\mathbf{r},\omega,S) = \mathbf{H}_n(\mathbf{r},\omega) + \sum_k S_{ak}\ \mathrm{curl}(\mathbb{G}(\mathbf{r},P_k,\omega))\, \mathbf{E}(P_k,\omega,S(\mathbf{r}'))\, |P_k| \quad (5)$$

at any point $\mathbf{r}$ and any frequency ω.

Let us consider the linear system made up of equation (4) written at each point P_k of Ω, $k = 1,\ldots,K$. Given the distribution of anomalous conductances S_{ak}, $k = 1,\ldots,K$, the quantities $\mathbf{E}(P_k,\omega,S(\mathbf{r}'))$ are solutions of this system. For each frequency, the system has $6 \times K$ equations and $6 \times K$ real unknowns in the general case. Solving this system allows us to compute the electric field $\mathbf{E}(\mathbf{r},\omega,S(\mathbf{r}))$ at any point $\mathbf{r}$ and frequency ω. The magnetic field $\mathbf{H}(\mathbf{r},\omega,S(\mathbf{r}))$ is then derived using (5) written at any point $\mathbf{r}$ and frequency ω.

5.4 The inverse problem

The structure of the embedding 1-D model, i.e., $S_n(\mathbf{r})$, the depth of the heterogeneous thin sheet, the domain Ω, and the cells P_k are first defined, and remain fixed during the inversion. Their values are to be deduced from previous investigations in the studied area (geology, other geophysical methods, ...) and from laboratory measurements of rock conductivity. The conductances S_k, $k = 1,\ldots,K$, are the parameters, and solving the inverse problem consists in estimating their a posteriori *pdf* given the data $\mathbf{d} = (d_{ij})$, $i = 1,\ldots,I$, $j = 1,\ldots,J$, and the a priori *pdf* P_0.

The data $\mathbf{d}$ are actually estimates of a function $\mathbf{T}\,[\,\mathbf{E}(\mathbf{r},\omega,S(\mathbf{r})),\mathbf{H}(\mathbf{r},\omega,S(\mathbf{r}))\,]$ at points $\mathbf{r}_i$, $i = 1,\ldots,I$, of the surface and frequencies ω_j, $j = 1,\ldots,J$, plus an experimental noise $\delta\mathbf{d}$,

$$d_{ij} = T\,[\,\mathbf{E}(\mathbf{r}_i,\omega_j,S(\mathbf{r})),\mathbf{H}(\mathbf{r}_i,\omega_j,S(\mathbf{r}))\,] + \delta d_{ij}. \quad (6)$$

The δd_{ij}, and therefore the d_{ij} are assumed to be independent gaussian random variables with zero mean value and standard deviation τ.

In situations for which no particular information is available, we choose as a priori distribution the product of a uniform *pdf* on each layer. In this case P_0 is a uniform distribution over all the possible models and where the different parameters are independent. P_0 is digitised over a set of conductance values, hereafter called possible conductance values, the choice of which depends on the a priori knowledge of the considered medium. There is no constraint on this choice, but it is clear that the larger this number the better the determination of the a posteriori distribution, but the greater the computer time. The possible conductance values may depend on the cell. We will only consider here situations with the same number L of possible values S_l, $l = 1,\ldots,L$, for each cell. The a posteriori distribution will accordingly be expressed as the a posteriori probability of these possible conductance values.

The a posteriori *pdf* of the parameters S is estimated by means of a Markov chain. Let an algorithm that considers each cell P_k successively and updates the value of the parameter for this cell with a transition probability equal to the conditional probability distribution of S_l, $l = 1,\ldots,L$, given the actual values of the parameters for the other cells, the data $\mathbf{d}$ and the a priori *pdf* $P_0(S)$. The sequence of images thus obtained after each scanning of the whole set of K cells is a homogeneous Markov chain, because the probability of an image depends only on the previous image, and does not change with step n. This process is a Markov chain on $\mathcal{M}$ called the Gibbs sampler (Robert, 1996). It is ergodic, and its invariant probability Π is the a posteriori probability is the conditional probability $\Pi(S)$ of the parameters given the data $\mathbf{d}$ and the a priori *pdf* $P_0(S)$ (Roussignol *et al.*, 1993; Roussignol and Menvielle, 1995; Robert, 1996; Grandis *et al.*, 1999; 2002).

In the present case, the required $L \times K$ solutions of the forward problem that are necessary for computing the transition probability of the Markov chain (in the present case, the K conditional *pdf*'s corresponding to the whole set of cells) requires a very long CPU time. In order to limit the CPU time, the forward problem is not fully solved at each scanning, and the electric field is estimated by the Markov chain. The Markov chain is then a two-dimensional one, which estimates a quantity (the conductance) distributed over a finite set of real values and another one (the electric field) distributed over a continuous set of real vectors.

The asymptotic behavior of such a Markov chain has first been studied empirically by Jouanne (1991), then Grandis (1994) for situations representatives of those encountered in geophysics. Using synthetic models, Grandis (1994) evidenced that the empirical average of the transition *pdf* of this Markov chain tends towards an invariant *pdf* that corresponds to the a posteriori *pdf* of the parameters, provided the estimate of the electric field at each scanning is precise enough for the transition probabilities to be reasonably estimated. Later on, Touijar (1994) gave the first demonstration that such a chain converges under given conditions. The physical interpretation of Touijar's mathematical results suggests that the empirical results established by Jouanne (1991) and Grandis (1994) are likely to be valid for most of geophysical situations (Menvielle and Roussignol, 1995).

6 The inversion

6.1 The description of the model and data

In accord with the above discussion, we chose the following particular parameters for the thin sheet model used in the MCMC inversion of the long-period geomagnetic induction data over the BM/BV/WCP region:

(i) The anomalous domain of the superficial thin sheet is divided into 21(N)×29(E) square cells, each 25×25 km^2 in size, covering thus a region of about 500(N)×750(E) km^2. This gives in total 609 variable parameters (cell conductances) for the inversion.

(ii) The normal model was composed of a two-layer background model with the first layer of 100 km/1000 Ωm and a uniform basement of 300 Ωm. The basement was used to simulate the asthenospheric layer. The topography of the asthenosphere was neglected. The layered model was overlain by a uniform infinite thin sheet with the conductance of 300 siemens.

(iii) For the inversion purposes, the 150 experimental geomagnetic TF's available were interpolated into the centers of the sheet cells. As reliable data variances were not available for the experimental TF's, we assumed the data to be contamined with Gaussian errors with the standard deviation of 0.03.

(iv) For the MCMC run, data for only one period, $T = 3860$ s, were used to keep the computation times in reasonable limits. Fit of the data and model arrows for further periods available were only checked by direct modeling tests.

6.2 The MCMC procedure, convergence, output models, post-processing

For the MCMC procedure (Gibbs sampler), the conductance of each of the 609 variable cells could take on one of 12 predefined values from the interval of 3 to 5000 siemens. The Markov chains were typically running for 1000 cycles of the Gibbs sampler, which took about 10 hours of the CPU time on a standard PC station (Intel Xeon 3 GHz, 1 MB RAM). Repeated MCMC runs were carried out to simulate parallel chains and check the convergence of the MCMC process. First 500 cycles of each of the MCMC chains were discarded as a burn-in period during which the chain approaches a vicinity of the solution and stabilizes. In our runs, the chains did not change substantially after the burn-in period, and simulated parallel chains converged to similar conductance distributions for the same cells. From this rough diagnostics, we can conclude that the chains converged and can provide reasonable estimates of the means of the cell conductances within the selected model class $\mathcal{M}$. As the number of MCMC iteration cycles is relatively small in our experiments, it is not realistic to obtain reasonably accurate estimates of higher moments of the aposteriori *pdf*'s for the cell conductances. In fact, only highly qualitative conclusions may be made as regards the uncertainties of the variables.

The MCMC procedure gives a series of models which should be probabilistically distributed in accord with the experimental data. We obtain a whole histogram of conductance values for each cell, which shows how much likely are the particular conductance values in the cell considered. After long enough iteration process, the histograms approximate the marginal aposteriori probabilities of the discrete conductance values in the individual sheet cells. We can estimate the mean values of the cell conductances by integrating over the histogram, as well as the most probable cell conductances (maximum aposteriori probabability, or MAP estimates) by taking the most frequent value from the histogram.

Fig. 3 displays sheet models over the BM/BV/WCP region set together from the mean values of the conductance in the individual sheet cells and from the MAP estimates of the cell conductances. These models do not represent the average or MAP models from the chain, which would both require integration of the multi-dimensional empirical posterior *pdf* over the whole parameter space. The presented models are put together from estimates based on individual marginal *pdf*'s for the individual sheet cells. It is clear that these models may differ considerably from each other, especially in regions where the cell conductances are poorly constrained by the data. Nevertheless, the models in Fig. 3 represent simple integrated information on the conductance structure projected from a 3-D probabilistic (histogram) image of the cell conductances provided by the whole underlying Markov chain. Fit of the model data from the 'average' model in Fig. 3 (left) and the experimental induction arrows is shown in Fig. 4 for the inverted period of 3860 s. Model vs. experiment fit for longer periods (not shown) is very similar, larger discrepancies are observed for the period $T = 1200$ s with model induction arrows substantially smaller than the experimental data. This is most likely due to a misspecified depth of the sheet in our model (superficial sheet).

Qualitatively, we can also estimate the uncertainty of the conductance by simply observing the 'flatness' or 'peakiness' of the histograms for the cell conductances. In Fig. 5 (left), we show the 'average' model from Fig. 3 (left) modified by keeping in it only those cells for which 90% of the cell conductance values in the MCMC histograms fall within an interval of a width of 2/3 of a decade. All remaining cells, with flatter conductance histograms, have been discarded. The cells in Fig. 5 (left) thus indicate regions of the model in which the conductance is reasonably well constrained by the data. More precise, quantitative uncertainty estimation would be perhaps possible from longer MCMC

chains which would allow us to integrate directly for variance-covariance functions estimates for the parameters.

Because of high computational demands, thin sheet models for the MCMC inversion are mostly designed with only a coarse tiling. In the model post-processing stage, spatial smoothing often results in a more realistic image of the conductance distribution. The smoothed image has to be checked by an additional direct modeling test. We show a smoothed version of the 'average' conductance model from Fig. 3 (left) in the right-hand side panel of Fig. 5.

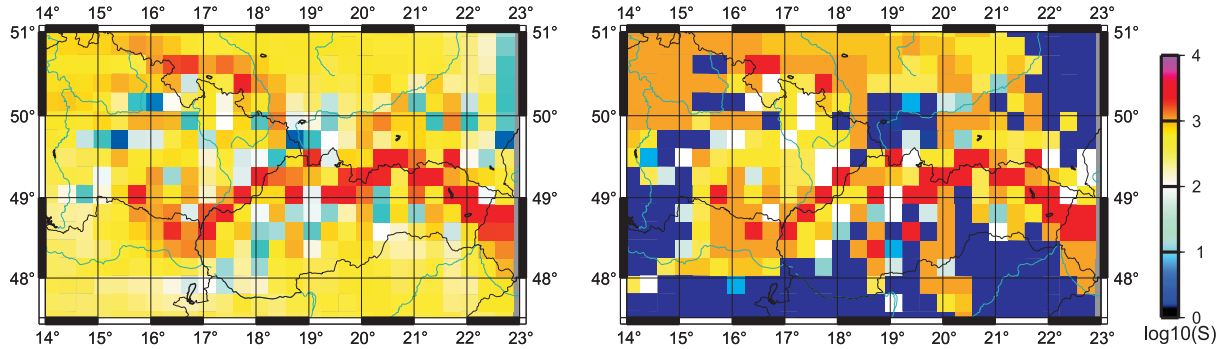

Figure 3: Left: Conductance model over the BM/BV/WCP region designed from average cell conductances obtained form the stabilized part of the Markov chain. Right: Conductance model designed from maximum aposteriori conductances in the individual sheet cells. The color scale corresponds to the logarithm of the conductances. Period of inverted data was 3860 s.

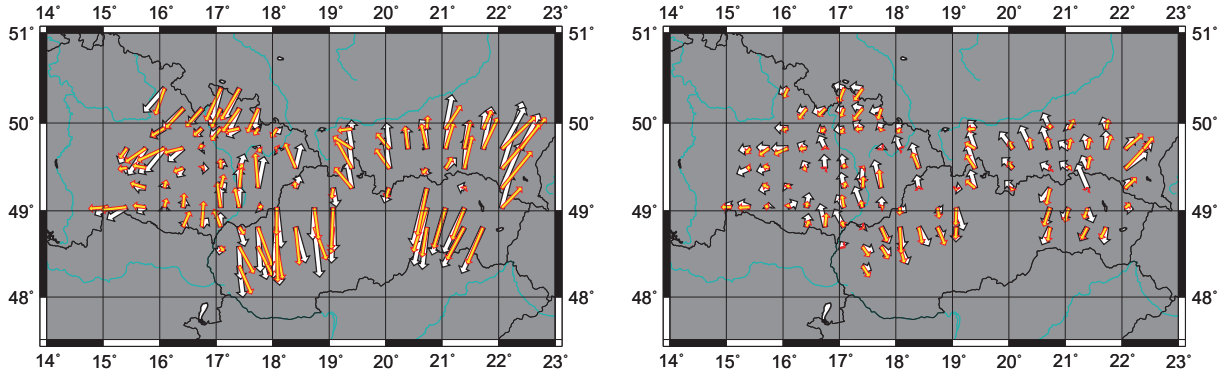

Figure 4: Fit of the real (left) and imaginary (right) induction arrows for the period of 3860 s. White arrors show the input data obtained by interpolating the experimental TF's into the centers of the sheet cells. Orange-yellow arrows were generated by the thin sheet model designed from average cell conductivities from the MCMC chain (model to the left in Fig. 3).

7 Tectonic correlation

Interpretation of narow-band long-period geomagnetic data by the MCMC sampling can only provide a large-scale image of the conductance distribution which conforms with the observed TF's. The conductance pattern restored from the induction arrows collected above the eastern slopes of the BM and its transition to the WCP gives a geologically plausible image of the region. The Carpathian conductivity anomaly is reconstructed in detail, suggesting possible weakening/local interruption at the crossing with the Central Slovakia fault zone (near 19.2^{o}E in Fig. 5 right) where other geophysical fields and geological indicators show discontinuous features on a presumably strike-slip fault (e.g., Kováč and Hót, 1993). Though in coarse mesh, the high conductance anomaly well fits the position of a low resistivity layer from the magnetotelluric data collected in the esternmost sector of the model, close 22^{o}E (Vozár, 2005).

The induction anomaly at the eastern margin of the Bohemian Massif seems to have a more complex explanation than that of a quasi-linear conductor along the SW-NE zone of a rapid change of direction of the induction arrows (see Fig. 2). Two features may be observed in the model in Fig. 5 (right), which were already discussed earlier by Kováčiková *et al.* (2005). First, it is a conductive zone in the NE of the BM, which may generate induction arrows directed towards the SW, as clearly observed all across the area to the west of the EBMA. Second, it is an alteration of conductive and resistive E-W zones in the eastern part of the BM. Though still not clear how much of this effect

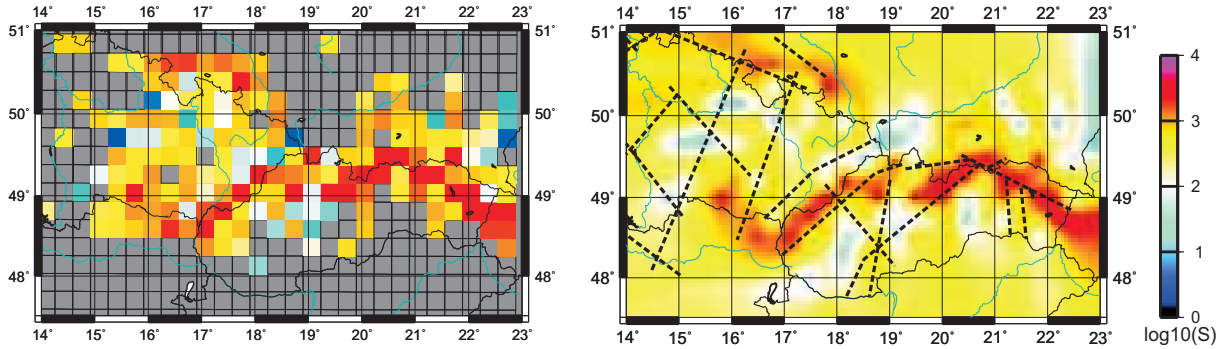

Figure 5: Left: Model from Fig 3 (left) with only those cells of the original 'average' model shown that have 90% of all conductance values within 2/3 of a decade. Cells with flat histograms are eliminated. Right: Spatially smoothed 'average' conductance model. The dashed lines indicate main regional fault zones.

may be caused by the profile arrangement of the data, this quasi-anisotropic domain is actually required by the data. It helps in feeding the induction process all across the Moravia region and in keeping the relatively large modules of the induction arrows in that region. If these induction sources could be verified, the regional induction in the eastern part of the BM would be mainly driven by the NW-SE to W-E pattern of tectonic zones (Elbe fault zone, Sudety faults, Poříčí-Hronov fault zone, Odra fault zone, etc.) rather than by the SW-NE zones which conform with the tectonics of the transition to the WCP.

8 Conclusion

From the experience accumulated with the MCMC inversion we can conclude that for moderately sized thin sheet models (tens of cells in each direction), the MCMC inverse procedure is practicable with standard computer facilities. Speeding-up the forward solutions by using a 2-D Markov chain derived from the integral equation numerical approach by Vasseur and Weidelt (1977) is essential for the algorithm.

Though computationally still demanding, the advantage of the MCMC is that it provides a probabilistic output for the inverse solution. Parameters can be assessed with respect to their values and uncertainty ranges, though true uncertainties (variance-covariance matrices) are hard to obtain in problems with demanding direct solutions. Effective visualization of complete probabilistic outputs from the MCMC algorithm may still be one of its weak points.

The conductance pattern restored by the MCMC sampling from the induction arrows collected above the eastern slopes of the BM and its transition to the WCP gives a geologically plausible image of the region. The Carpathian conductivity anomaly is reconstructed in detail. The induction anomaly suggested at the eastern margin of the BM admits an alternative explanation in terms of a NW-SE to W-E conductance patterns, hypothetically coinciding with the fault pattern of the eastern Bohemian Massif. A detailed verification of the structural hypotheses in this region is, however, hardly possible by employing the long period geomagnetic induction data alone.

Acknowledgements

Financial assistance of the Czech Sci. Found., contract No. 205/07/0292, and of the Grant Agency Acad. Sci. Czech Rep., contract No. IAA300120703, is highly acknowledged.

References

Ádám, A., 1976. Results of deep electromagnetic investigations. In: Ádám (Editor), Geoelectric and Geothermal Studies, KAPG Geophysical Monograph, Akadémiai Kiadó, Budapest, 547-559.

Ádám, A. and Pospíšil, L., 1984. Crustal conductivity anomalies in the Carpathian region. Acta Geodaet. Geophys. Montanist. Hung., 19, 19-34.

Ádám, A., Landy, K. and Nagy, Z., 1988. New evidence for the special distribution of the electric conductivity in the Earth's crust and upper mantle in the Pannonian basin as a 'hot spot', Tectonophysics, 164, 361–368.

Babuška, V., Plomerová, J. and Pajdušák, P., 1988. Lithosphere-asthenosphere in Central Europe: Models derived from P-residuals, in Proceedings of the Fourth Workshop on the European Geotraverse (EGT) project: The Upper Mantle, G. Nolet and B. Dost (Eds.), ESF, Strasbourg, 37-48.

Berger, J. O., 1985. Statistical Decision Theory and Bayesian Analysis, Springer-Verlag, New York.

Bolstad, W. M., 2004. Introduction to Bayesian Statistics, John Wiley & Sons, 2004.

Box, G. and Tiao, G., 1973. Bayesian Inference in Statistical Analysis, Addison-Wesley, Reading.

Bruton P., 1994. Testing Vasseur and Weidelt's thin sheet algorithm, in Proceedings of the 15th Colloquium 'Electromagnetic Depth Research', Bahr, K. and Junge, A. (Eds.), DGG, pp. 54-59.

Červ, V. and Pek, J., 1981, Numerical solution of the two-dimensional inverse geomagnetic induction problem. Studia geoph. et geod., 25, 69-80.

Červ, V., Pek, J. and Praus, O., 1984. Model of geoelectrical anomalies in Czechoslovakia. J. Geophys., 55, 161-168.

Červ, V., Pek, J. and Praus, O., 1987.Numerical modelling of geoelectrical structures in Czechoslovakia. Phys. Earth Planet. Inter., 45, 170-178.

Červ, V., Pek, J. and Praus, O., 1990. Limitations of the unimodal thin sheet modelling of near-surface inhomogeneities in Czechoslovakia, Phys. Earth Planet. Inter., 60, 100-114.

Červ, V., Kováčiková, S., Pek, J., Pěčová, J. and Praus, O., 1997. Model of Electrical Conductivity Distribution across Central Europe, J. Geomag. Geoelectr., 49, 1585-1600.

Dudek, A., The crystalline basement block of the Outer Carpathians in Moravia: Brunovistulicum, Ropr. Cs. Akad. Ved, R. mat. a pr. ved, Praha, 90, 1980, 1-85.

Glover, P.W.J. and Vine, F.J., 1992. Electrical conductivity of carbon-bearing granulite at raised temperatures and pressures, Nature 360, 723-726.

Glover, P.W.J. and Vine, F.J., 1995. Beyond KTB-Electrical conductivity of the deep continental crust, Surveys in Geophysics, 16, 5-36.

Grandis, H., 1994. Imagerie electromagnetique Bayesienne par la simulation d'une chaine de Markov, Doctorat d'Université, Université Paris VII.

Grandis, H., Menvielle, M. and Roussignol, M., 1999. Bayesian inversion with Markov chains—-I. The magnetotelluric one-dimensional case, Geophys. J. Int., 138, 757–768.

Grandis, H., Menvielle, M. and Roussignol, M., 2002. Thin-sheet electromagnetic inversion modeling using Monte Carlo Markov Chain (MCMC) algorithm, Earth Planets Space, 54, 511–521.

Hvoždara, M. and Vozár, J., 2004. Laboratory and geophysical implications for explanation of the nature of the Carpathian Conductivity Anomaly. Acta Geophysica Polonica, Vol. 52, No. 4, pp. 497-508.

Jankowski, J., Petr, V., Pěčová, J. and Praus , O., 1984. Geoelectric anomaly in the Czechoslovak-Polish section of the Carpathians on the basis of geomagnetic and magnetotelluric soundings, Acta Geodaet., Geophys. Montanist. Hung., 19, 81-91.

Jankowski, J., Tarlowski, Z., Praus, O., Pěčová, J. and Petr, V., 1985. The results of Deep Geomagnetic Soundings in the West Carpathians, Geophys. J. Royal Astron. Soc., 80, 561-574.

Jankowski, J., Pawliszyn, J., Jóźwiak, W. and Ernst, T., 1991. Synthesis of electric conductivity surveys performed on the Polish part of the Carpathians with geomagnetic and magnetotelluric sounding methods, Publs. Inst. Geophys. Pol. Ac. Sci., A-19(236),183-214.

Jankowski, J., Jóźwiak, W. and Vozár, J., 2008. Arguments for ionic nature of the Carpathian electric conductivity anomaly, Acta Geophys., 56, 455-465.

Jouanne, V., 1991. Application des techniques statistiques Bayesiennes a l'inversion de données électromagnétiques, Doctorat d'Université, Université Paris VII.

Kováč, P. and Hók, J., 1993. The Central Slovak Fault System-=field evidence of a strike slip. Geol. Carpath., 44, 133-159.

Kováčiková, Červ, V., Praus, O., 1997. Modelling of geomagnetic transfer functions on the eastern margin of the Bohemian Massif, Annales Geophysicae, 15, Suppl. I, C 159.

Kováčiková, S., Červ, V. and Praus, O., 2005. Modelling of the conductance distribution at the eastern margin of the European Hercynides, Studia geophys. geod., 49, 403-421.

Menvielle, M. and Roussignol, M., 1995. Imagerie électromagnétique bayesienne. In: Munschy, M., Sauter, D., Schlich, R. (Eds.), Comité National Français de Géodésie et Géophysique, Rapport Quadriennal 1991–1994, Paris, France, pp. 177–190.

Pěčová, J. and Praus, O., 1996. Anomalous induction zones in the Czech republic in relation to large scale European anomalies, Studia geoph. et geod., 40, 50-76.

Praus, O., Pěčová, J., 1991. Anomalous geomagnetic fields of internal origin in Czechoslovakia, Studia geoph. et geod., 35, 81-89.

Praus, O., Pěčová, J., Petr, V., Babuška, V. and Plomerová, J., 1990. Magnetotelluric and seismological determination of the lithosphere-asthenosphere transition in Central Europe, Phys. Earth Planet. Inter., 60, 212-228.

Press, S.J., Flannery, B.P., Teukolsky, S.A. and Vetterling, W.T., 1989. Numerical Recipes: the Art of Scientific Computing, Cambridge University Press, Cambridge.

Robert, C., 1996. Méthodes de Monte Carlo par Chaines de Markov, Economica, Paris.

Roussignol, M., Jouanne, V.,Menvielle, M. and Tarits, P., 1993. Bayesian electromagnetic imaging, in Computer Intensive Methods, pp. 85–97, Hardle, W. and Siman, L. (Eds.), Physical Verlag.

Schott, J.-J., Roussignol, M., Menvielle, M. and Nomenjahanary, F. R., 1999. Bayesian inversion with Markov chains—-II. The one-dimensional DC multilayer case, Geophys. J. Int., 138, 769–783.

Suk, M., Blížkovský, Buday, M., Chlupáč, I., Cicha, I., Dudek, A., Dvořák, J., Eliáš, M., Holub, V., Ibrmajer, J., Kodym, O., Kukal, Z., Malkovský, M., Mencík, E., Müller, V., Tyráček, J., Vejnar, Z., Zeman, A., 1984. Geological history of the Czech Socialist Republic, Publ. of Ústřední ústav geologický, 17-86.

Suk, M., 1995. Regional geological division of the Bohemian Massif, Exploration Geophysics, Remote Sensing and Environment, II. 2., 25-30

Touijar D., 1994. Stochastic algorithms and application to Bayesian electromagnetic imaging, PhD Thesis, Travaux Universitaires–Thčse nouveau doctorat, Université de Lille 1, Villeneuve-d'Ascq, France, 104 pp.

Vasseur, G. and Weidelt, P., 1977. Bimodal EM induction in non-uniform thin sheets with an application to the Northern Pyrenean Anomaly, Geophys. J. R. astr. Soc., 51, 669-690.

Vozár, J., 2005. Magnetotelluric Soundings on the Territory of Slovakia, PhD Thesis, GFU SAV Bratislava, 2005, 108 pp. (in Slovak).

Wang, L. J. and Lilley, F. E. M., 2002. Inversion of magnetometer array data by thin-sheet modelling, Geophys. J. Int., 137, 128-138.

Weidelt, P., 1975, Electromagnetic induction in three-dimensional structures, J. Geophys., 41, 85-109.

Wiese, H., 1962. Geomagnetische Tiefentellurik Teil II: Die Streichrichtung der Untergrundstrukturen des elektrischen Widerstandes, erschlossen aus geomagnetischen Variationen, Geofisica pura e applicata, 52, 83-103.

Wybraniec, S., Jankowski, J., Ernst, T., Pěčová, J., Praus, O., 1999. A new method for presentation of induction vector distribution in Europe, Acta geophys. polonica, XLVII, 323-334.

Źytko, K., 1997, Electrical conductivity anomaly of the Northern Carpathians and the deep structure of the orogen, Annales Societatis Geologorum Poloniae, 67, 25-43.